RESEARCH PAPER

Effect of ZrO_2 Doping on the Properties of TiO_2 Thin Films as an Ethanol Vapor Gas Sensor

Zainab T. Hussain[1], Wasna'a M. Abdulridha[2], Murooj A. Abood[1], Farqad Rasheed Saeed[1,*]

* *farqad.r.saeed@src.edu.iq*

[1] Scientific Research Commission, Baghdad, Iraq
[2] Department of Basic science, University of Kufa, Faculty of Science, Najaf, Iraq

Received: March 2025 **Revised: December 2025** **Accepted: March 2026**
DOI: 10.22068/ijmse.3955

Abstract: *In this study, RF magnetron sputtering was employed to deposit titanium dioxide (TiO_2) thin films doped with zirconium oxide (ZrO_2) (TZO) onto quartz and silicon substrates at 100°C to evaluate the effect of ZrO_2 doping on the microstructural, electrical, optical, and gas-sensing properties of the TiO_2 films. Different doping concentrations (0.0, 2.0 and 4.0 wt%) were used; film thickness ranged from 147 nm to 179 nm. Structural and surface-morphology characterizations of the prepared films were carried out using X-ray diffraction (XRD) and atomic force microscopy (AFM). The surface morphology of the prepared TZO films showed a gradual reduction in grain size as the doping concentration increased. The optical properties exhibited an increase in the optical band gap with the increasing ZrO_2 concentration. Hall measurements confirmed n-type conductivity for the TiO_2 films. Gas-sensing experiments revealed that the sensitivity of the TZO films for ethanol vapor detection increased with ZrO_2 concentration. Therefore, a TZO film with 4.0 wt% ZrO_2 may serve as an effective ethanol-vapor sensor.*

Keywords: *Zirconium oxide, Titanium dioxide, RF sputtering, Thin film, Sensitivity, Sensor, Ethanol vapour.*

1. INTRODUCTION

Titanium dioxide (TiO_2) is a wide-band-gap semiconductor with notable properties. TiO_2 has a high refractive index, is non-toxic, and exhibits high chemical stability over a wide pH range and in various solvents [1]. TiO_2 is typically an n-type semiconductor due to oxygen vacancies and is widely used in many applications, including the food and pharmaceuticalindustries, photocatalysis, and hydrogen production; it is also suitable as a functional material for fuel cells, optical coatings, and solar cells [2]. Additionally, TiO_2 can be used as a substrate in gas sensors because of its chemical and thermal stability. Incorporation of selected elements into TiO_2 often improves its gas-sensing activity [3]. TiO_2 shows good sensing characteristics toward H_2, CO and ethanol [4, 5]. TiO_2 exists in several crystalline forms: anatase (tetragonal), rutile (tetragonal), and brookite (orthorhombic) [6]. At elevated temperatures, anatase commonly transforms to rutile [7]. The anatase phase is widely recognized as the most efficient photocatalyst because of its favorable electronic band structure and relatively slow recombination of photogenerated electron-hole pairs. Anatase has a larger band gap (~3.2 eV) than rutile (~3.0 eV), that making it more active under UV light [8, 9].

Several techniques have been used to synthesize TiO2 films, including electron-beam evaporation, liquid deposition, RF and DC sputtering, sol–gel and pulsed laser deposition [10–15]. The properties of TiO_2 films depend not only on deposition conditions but also on the preparation method [16]. TiO_2 has been modified by doping with N, Ag, P, and photosensitive dye molecules (e.g., porphyrins) [17–20], and by combining with other semiconductors such as ZnO [21], CeO_2 [22], SnO_2 [23], or ZrO_2 to improve specific surface area, photocatalytic activity, or reduce free-radical generation [24]. The aim of this research is to control the optical and structural properties of thin films deposited by RF sputtering (argon atmosphere, fixed substrate temperature) by varying ZrO_2 content. Among metal oxides, zirconium oxide (ZrO_2) exhibits high hardness and mechanical strength, a large band gap, high corrosion resistance, a high melting point, high refractive index, low thermal conductivity, and good oxygen-ion conductivity [25–27]. ZrO_2 can generate oxygen vacancies and has been described in some works as showing p-type behavior. Applications include thermal-barrier coatings, gas sensors, heat resistance in high-temperature furnaces, solar cells, biosensors, and oxygen sensors [28]. Because TiO_2 and ZrO_2 have similar physical and chemical properties, combining them can produce materials with

[DOI: 10.22068/ijmse.3955]

improved chemical stability, electrical and photocatalytic properties not achievable with a single oxide. TiO_2–ZrO_2 binary oxide coatings have been applied to electrochemical storage, antibacterial agents, gas sensing, and photocatalysis [29]. Binary metal-oxide coatings also tend to exhibit increased porosity and specific surface area, which can assist charge transport and inhibit recombination. The sol–gel technique has often been used to deposit such binary coatings [26], although other methods are also reported [30]. Magnetron sputtering has been less explored for TiO_2–ZrO_2 binary films despite its capability to produce dense, homogeneous coatings at nanometer scale when parameters (base pressure, purity, substrate temperature, deposition time, etc.) are optimized [31]. For example, MgO-doped TiO_2 films have been prepared by confocal sputtering and evaluated for gas sensing [32].

The researchers investigated the structural, morphological, and optical properties of the films and their gas sensor performance. Gas sensing measurements were performed at 300°C using methane gas, and the sensitivity and response/recovery time of the gas sensors were evaluated at 1000 ppm. The study found that the MgO doped TiO_2 sensor showed high sensitivity and short response/recovery time indicating an improvement in electrical and gas sensing performance.

There is growing demand for real-time, high-performance semiconductor gas sensors in industry. A binary oxide coating would form the core of a gas sensor. However, proportions of the oxide materials in the binary coatings and its gas sensing mechanism are still needed to be studied. Today, human activities driven by the increase in global industrial processes produce toxic chemicals, including toxic gases and volatile organic compounds (VOCs), which are among the main worldwide environmental issuesEthanol is an important volatile organic compound (VOC) widely used across industries such as beverages and fuel processing [33]. This work focuses on TiO_2 thin films. Therefore, this work was focused on TiO_2 thin films prepared by RF magnetron sputtering and evaluates the effect of ZrO_2 doping (0–4 wt%) on grain size, structure, and ethanol sensing at room temperature.

2. EXPERIMENTAL PROCEDURES

2.1. Materials

TiO_2 powder (99.99% purity) was used to fabricate targets for deposition. ZrO_2 powder (99.99% purity) was mixed with TiO_2 powder to prepare composite targets with 0 wt%, 2 wt% and 4 wt% ZrO_2. Pellets were prepared by compressing 30 g of powder under 10-ton compression at 80°C. For doped targets, the total mass was 30 g with the appropriate TiO_2:ZrO_2 ratios (98:2 and 96:4 for 2% and 4% TZO, respectively). The pellets measured 50 mm in height and 50 mm in diameter.

2.2. Procedure for Coating Deposition

TZO thin films were deposited by RF magnetron sputtering onto cleaned quartz and silicon substrates. Silicon substrates were used for electrical and gas-sensing characterization; quartz substrates were used for optical and microstructural studies. Substrates were ultrasonically cleaned in ethanol (99.99% purity) for 3 min at room temperature, rinsed several times with deionized water, then ultrasonically cleaned in deionized water for 5 min. Finally, argon gas was used to dry the substrates Quartz substrates measured 2.5 × 2.5 cm^2. The RF magnetron sputtering chamber (stainless steel) had a diameter of 230 mm and height of 250 mm (Figure 1). All substrates were placed on a circular holder (100 mm diameter). Argon (99.999% purity) was the working gas; the target-to-substrate distance was approximately 50 mm. After loading and cleaning, the chamber was evacuated to a base pressure of 5.5×10^{-5} mbar. Argon
flow (30 sccm) was introduced and the chamber pressure adjusted to 5×10^{-3} mbar. RF power was set to 100 W and sputtering proceeded for 60 minutes with the substrate temperature maintained at 100°C. Coatings were annealed in air at 500°C for 2 h in a muffle furnace to achieve crystallization, consistent with previous studies [34].

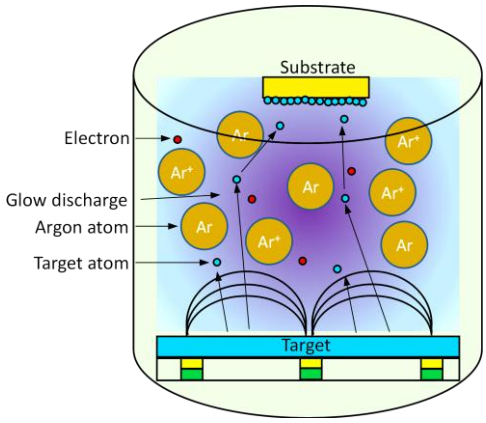

Fig. 1. RF magnetron sputtering deposition setup used to prepare TiO_2:ZrO_2 (TZO) thin films

[DOI: 10.22068/ijmse.3955]

2.3. Coating Characteristion Methods

Crystal structure was analyzed by X-ray diffraction (Shimadzu XRD-6000) in Bragg–Brentano geometry using Cu Kα radiation (40 kV, 30 mA). Scans were collected from 20° to 60° (2θ). Surface morphology was examined by atomic force microscopy (AFM, model A3000, Angstrom Advanced Lines, USA). Film thickness on glass substrates was measured by a Fizeau interferometer using a He–Ne laser (λ= 632.8 nm) and Equation (1):

$$T= (\lambda/2)(\Delta x/x) \quad (1)$$

Where it is the thickness of thin films, λ: is the laser wavelength (632.8 nm), e.g (Δx= 7) is the dark fringes, and (x= 1.5) is the bright fringes. Sputtered thin films on glass substrate have a thickness of between (147.6-178.8) nm with different doping. where T is film thickness, λ is the laser wavelength (632.8 nm), Δx is the number of dark fringes and x is the number of bright fringes. Sputtered thin films on glass had thicknesses between 147.6 nm and 178.8 nm for different dopings. Optical properties were measured with a UV–Vis spectrophotometer (Shimadzu 3600) in the 300–900 nm spectral range. Absorbance and band-gap calculations follow methods described by the authors previously [32]. Electrical properties (sheet resistance, carrier type and mobility) were measured using the van der Pauw method with an HMS-3000 Hall effect measurement system, a Keithley 220 current source and a Keithley 195 A digital multimeter. Overall sheet resistance was also confirmed using a Keithley 2636 System SourceMeter® [32].

2.4. Ethanol Gas Sensing Test Procedure

Ethanol (C_2H_5OH) sensing properties of pure TiO_2 and TZO samples were evaluated using a custom test chamber (30 × 40 × 30 cm^3) equipped with a rotary vacuum pump (EDM12, Edwards, UK) capable of 1.33×10^{-5} bar, and pressure and flow controllers. First, sensor resistance was measured in ambient air. Ethanol vapor was generated by heating liquid ethanol to 200°C and introduced into the chamber through a valve. A bias voltage of 3 V was applied between the sensor electrodes, and an ethanol concentration of 30 ppm was maintained at room temperature by a needle valve. Measurements were performed at ambient laboratory conditions (relative humidity ≈45 ± 5%). A planar interdigitated electrode configuration was used to increase the effective electrode area and improve sensitivity. Resistance variation was recorded using a digital multimeter interfaced to a computer. Dry air was supplied via a flow meter and needle valve to ensure stable flow. After opening the gas inlet, the sensor resistance in gas (Rg) was allowed to stabilize; then the chamber was purged and resistance recovery in air (Ra) was recorded. Figure 2 shows a schematic of the gas-sensor testing system.

Sensor sensitivity (S) was defined as the normalized change in resistance per concentration and computed using Equation (2) [35, 36]:

where Cg is gas concentration.

$$S= [(R_a/R_g)\times100\%]/C \quad (2)$$

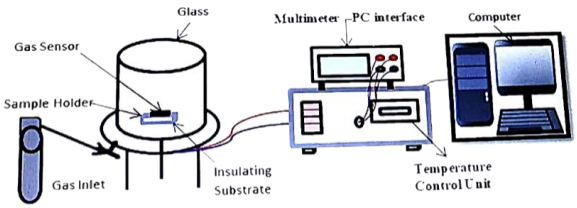

Fig. 2. Ethanol gas sensor testing system

3. RESULTS AND DISCUSSION

3.1. Crystalline Structure

Figure 3 shows XRD patterns of pure TiO_2 films and TZO films deposited on Si(100) at 100°C with 0.0, 2.0 and 4.0 wt% ZrO_2. As reported in [37], as-deposited (unannealed) TiO_2 exhibited an amorphous phase. After annealing at 500°C, TiO_2 films showed polycrystalline anatase phase (JCPDS 21-1272) with peaks at 25.25°, 37.8° and 48.05°, corresponding to the (101), (004) and (200) planes, respectively [38]. Sharp peaks in the pure TiO_2 film indicate high crystallinity and purity. The TZO films exhibited the same anatase diffraction peaks but with reduced intensity, possibly due to ZrO_2 incorporation into the TiO_2 lattice [39]. Doped TZO films also show weak peaks at 30.5° and 50.9° attributed to the (111) and (220) anatase planes (JCPDS 37-1484); the intensities of these peaks decreased with increasing ZrO_2 concentration. Peak intensities of TZO (2.0 wt% and 4.0 wt%) diminished as crystal size decreased to the nanometric scale, and peak broadening increased relative to pure TiO_2. Peak width correlated inversely with nanocrystalline domain size [40, 41]. These effects can be attributed to substitution of smaller Ti^{4+} ions (0.064 nm) by larger Zr^{4+} ions (0.087 nm), causing lattice distortion in anatase TiO_2 [39, 42]. Mean crystalline domain size (D) was estimated using the Scherrer equation [43]:

$$D= \frac{K\lambda}{\beta \cos\theta} \quad (3)$$

[DOI: 10.22068/ijmse.3955]

where λ is the X-ray wavelength, β is the full width at half maximum (FWHM) in radians after instrumental broadening correction, K= 0.9, and θ is the Bragg angle.

3.2. Surface Characteristics and Grain-Size Determination

Figure 4 shows 3D AFM images of TZO thin films deposited on glass at 0.0, 2.0 and 4.0 wt% ZrO_2.

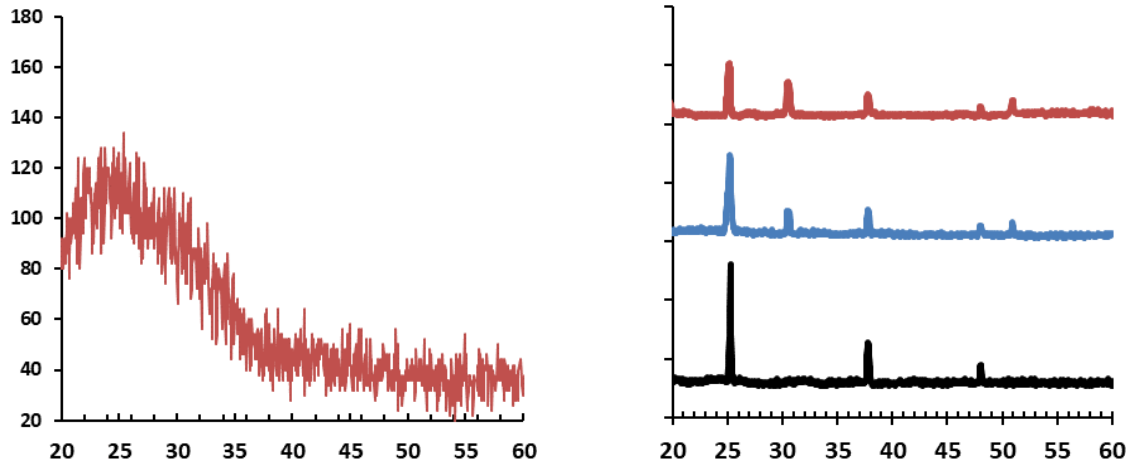

Fig. 3. XRD patterns of a) unannealed pure TiO_2 and b) TZO films with different ZrO_2 dopings annealed at 500°C

Table 1. Average grain size and roughness for TiO_2:ZrO_2 films on glass substrates

Coating name	ZrO_2 doping concentration (wt.%)	Average roughness grain size (nm)	(nm)
TiO_2 (pure)	0.0	99.3 ± 21 (nm)	1.1
TZO 2%	2.0	82.72 ± 17(nm)	5.37
TZO 4%	4.0	66.1 ± 11 (nm)	6.13

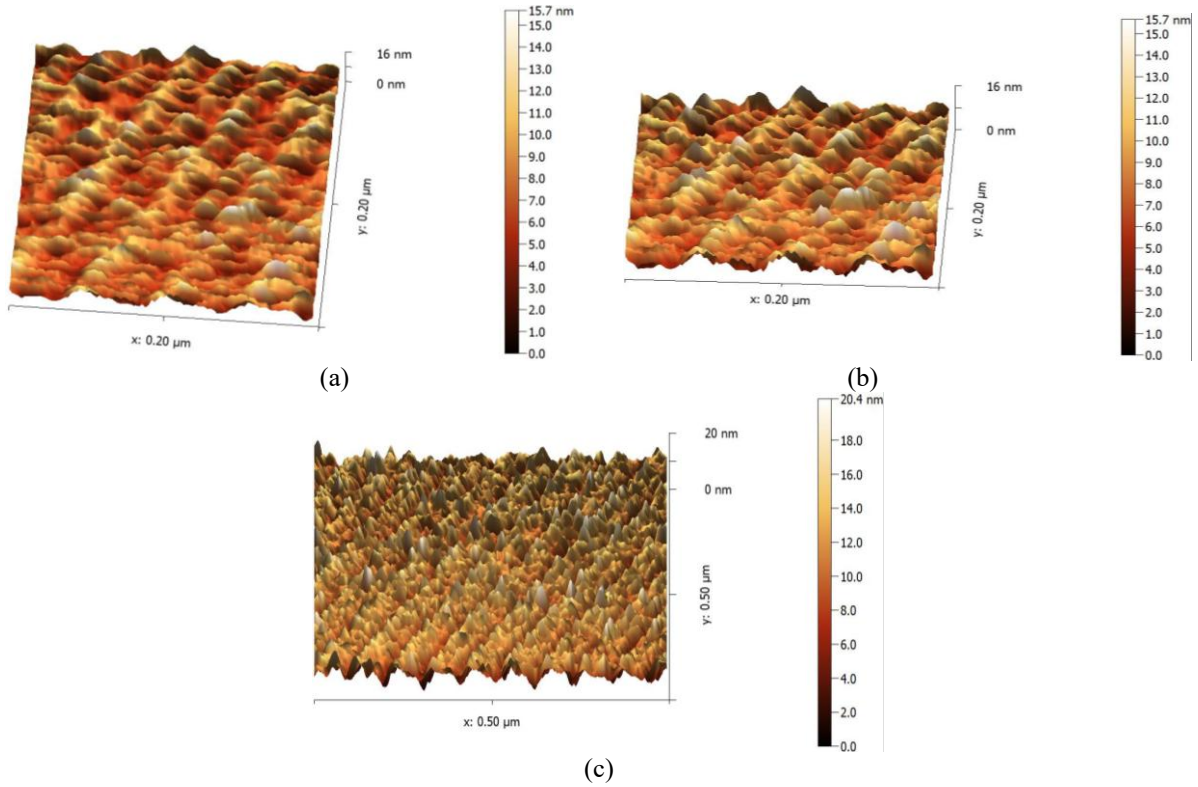

Fig. 4. 3D AFM images of a) TiO_2 (pure), b) TiO_2:ZrO_2 (2.0 wt%) and c) TiO_2:ZrO_2 (4.0 wt%) annealed at 500°C

[DOI: 10.22068/ijmse.3955]

The surfaces of annealed TiO_2 and TiO_2:ZrO_2 films were smooth and crack-free over large areas. Grain size of TiO_2 nanoparticles decreased after adding ZrO_2 [44]. Table 1 shows that TiO_2 doped with ZrO_2 had smaller average grain size than pure TiO_2; the grain size decreased with increasing ZrO_2 concentration. This trend is attributed to the formation of larger clusters by grain aggregation being suppressed, resulting in finer grains [45, 46]. Smaller grain size increases specific surface area and thus enhances gas-sensing performance [40].

3.3. Optical Properties

Figure 5 shows optical transmittance of TiO_2 and TZO films on quartz substrates in the 300–900 nm range. All films exhibited high transparency above 400 nm. The pure TiO_2 film had transmittance >75% in the visible region, whereas the 4.0 wt% TZO film showed lower transmittance (~33%). Between ~350 nm and 700 nm, clear differences in transmittance reflect the effect of ZrO_2 addition. Transmittance is also inversely related to film thickness and to changes in crystalline structure, where increased atomic density can raise absorbance and decrease transmittance [47].

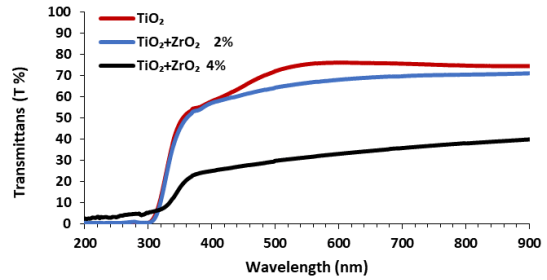

Fig. 5. Transmittance of TiO_2:ZrO_2 films as a function of ZrO_2 concentration

To measurement the thickness of deposited thin films by RF magnetron sputtering on the glass substrate by interferometer principle with He-Ne laser (632.8 nm). This process begins by directing laser beam (He-Ne) through a lens (F= -10) to expand the beam, the light of laser falls at 45° onto the deposited films. Due to light reflecting off both the top and bottom of thin film surface, when wave interference occurs, the bright and dark fringes appear. Determine the width of dark (Δx), and bright (x) fringes, by using equation (1) to calculated thickness of thin films. Table 2. Show the thin films thickness for TiO_2(pure), and TiO_2:ZrO_2 films deposited on glass substrate.

The direct optical band gap was estimated by plotting $(\alpha h\nu)^2$ versus photon energy ($h\nu$) and extrapolating the linear portion of the absorption edge [48, 49]. With increasing ZrO_2 concentration, the band gap of doped TZO films increased slightly up to ~3.4 eV (Figure 6), compared with undoped TiO_2; this increase is attributed to the presence of ZrO_2 and smaller grain size. The Tauc relation for direct transitions was used:

$$(Ah\nu)^2 = A(h\nu - Eg) \quad (4)$$

where α is the absorption coefficient, h is Planck's constant, A is a constant and Eg is the optical band gap [50, 51].

Therefore, it is clear that optical band gaps shifted towards longer wavelengths for the samples with increasing amount of ZrO_2 concentration. The TiO_2 materials are excited producing photo generated electrons and holes. Zirconia, with a larger band gap, is poorly activated but electrons from its valence band can be transferred to the valence band of TiO_2 as the energy levels are close to lower band gap [36, 37]. It should be acknowledged that the even though the band gap energies increased with the increasing concentration of ZrO_2 doping. This behaviour can be attributed to the state under Fermi level was occupied by electron, and at heavily doped Fermi level will enter the conduction band [52, 53]. In addition, the energy band gap of sample can affect by the impurities, disorder at the grain boundaries, stoichiometry and other defects, that which increase the optical band gap with the decrease of particle size. The presence of defects in the nanostructure thin films produces discrete states in the band structure [54].

3.4. Electrical Properties

Figure 7 shows the dependence of electrical resistivity and carrier mobility on ZrO_2 concentration for TiO_2:ZrO_2 films. The electrical resistivity decreased from 1.2×10^7 Ω·cm (pure TiO_2) to 7.93×10^4 Ω·cm at 4.0 wt% ZrO_2.

Table 2. Thickness for TiO_2:ZrO_2 films deposited on glass substrate

Coating name	ΔX (mm)	X (mm)	Thickness (T) (nm)
TiO_2 (pure)	0.7	1.5	147.6
TZO 2%	1.1	2.1	165.7
TZO 4%	1.3	2.3	178.8

[DOI: 10.22068/ijmse.3955]

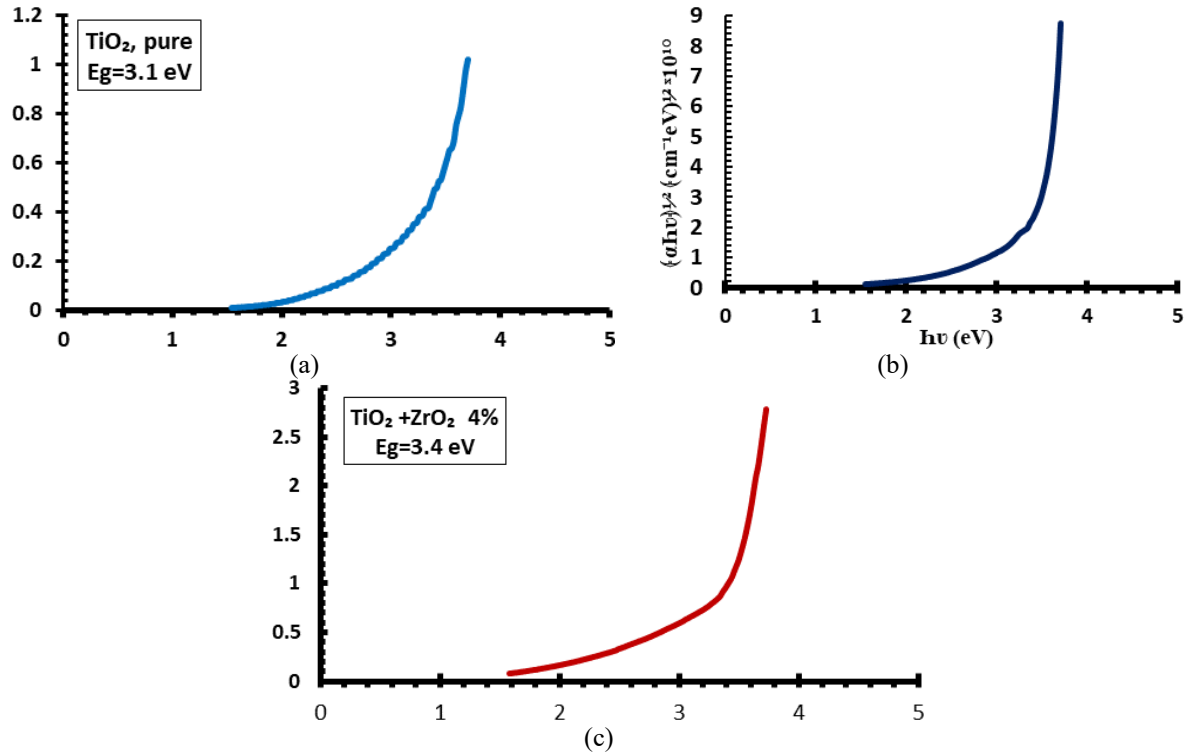

Fig. 6. The optical band gap of a) TiO_2 (pure) b) TiO_2:ZrO_2 (2.0 wt.%) and c) TiO_2:ZrO_2 (4.0 wt.%) annealed at 500°C

This decrease may be due to increased carrier concentration as extrinsic ZrO_2 substitution donates electrons to the TiO_2 host lattice [55]. Carrier mobility increased from 1.66 $cm^2V^{-1}s^{-1}$ (pure) to 46.7 $cm^2V^{-1}s^{-1}$ (2.0 wt%) and 736.2 $cm^2V^{-1}s^{-1}$ (4.0 wt%). Hall measurements indicate n-type conductivity [54]. Exposure of TiO_2:ZrO_2 sensors to ethanol vapor produced a larger decrease in resistance than for pure TiO_2 sensors. Electrical resistivity correlated.

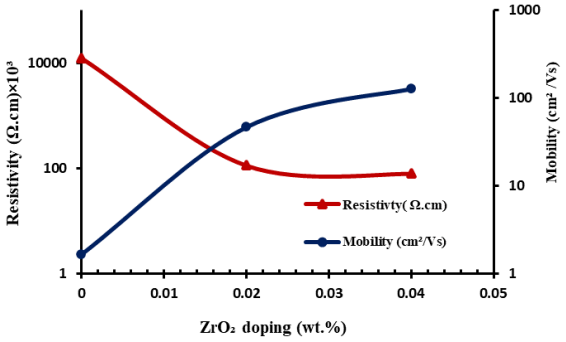

Fig. 7. Resistivity and mobility of TiO_2:ZrO_2 films as a function of ZrO_2 doping

As can also be seen in this figure, the electrical resistivity is inversely proportional to the carrier mobility, with the pure TiO_2 films having the highest resistivity as a result of low carrier concentration. Through doping, host TiO_2 sites were substituted by extrinsic ZrO_2, which provided an extra electron, thereby increasing the carrier concentration [55].

3.5. Gas Sensitivity of TiO_2 and TZO Thin Films

The sensing mechanism for ethanol (C_2H_5OH) involves adsorption and reaction of oxygen species on the film surface, which alters the film resistance. Adsorbed oxygen captures electrons from the conduction band to form ionic oxygen species; subsequent reaction with reducing gases (ethanol) releases electrons back, changing resistance. The resistance changes in the n-type such as, TiO_2, and TZO gas sensors at exposure to the reducing gas such as ethanol. The adsorption of oxygen molecules after their ionization causes a hole accumulation on the material's surface, lowering the resistance of the gas sensor [45]. Controlling particle size is critical because sensing reactions occur primarily at the surface; nanosized grains provide higher specific surface area and more active sites. The maximum sensitivity of pure TiO_2 in this study was ~5.11%/ppm (Figure 8 Sensitivity increased from 5.38%/ppm to 5.83%/ppm as ZrO_2 concentration increased from 2.0 wt% to 4.0 wt%. The films here achieved notable sensitivity at room temperature

[DOI: 10.22068/ijmse.3955]

compared to similar coatings prepared by inkjet printing that operate between 400–450°C [34].

The improvement in sensitivity with ZrO_2 doping is attributable to reduced particle size (82.7 nm → 66.1 nm), i.e., increased specific surface area and a higher number of adsorption sites [40]. In air, adsorbed oxygen forms O^- species that react with ethanol molecules, leading to increased surface electron concentration and improved sensing performance. The composite TiO_2–ZrO_2 sensor exhibits a smaller grain morphology and more oxygen-deficient sites compared to pure TiO_2.

An increased optical band gap with ZrO_2 doping may also correlate with enhanced sensing via grain-size reduction and increased surface area [40]. Because film thickness varied only slightly (147.6–178.8 nm), thickness is not expected to be a dominant factor in the observed sensing differences.

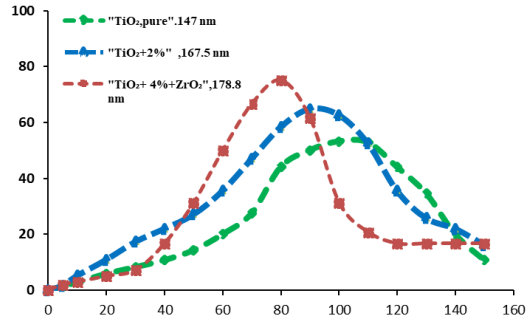

Fig. 8. Sensitivity of TiO_2:ZrO_2 films as a gas sensor at different doping

Response time (time to reach 90% of the maximum change in resistance after gas exposure) decreased from 85 s (pure TiO_2) to 45 s (4.0 wt% ZrO_2) at room temperature (Figure 9). Increased doping likely increases the availability of adsorption sites and accelerates reaction kinetics, resulting in faster responses. This could be explained by the rise in doping quantity increasing the availability of unoccupied sites on the thin films for gas adsorption. Therefore, with 4.0 wt.% ZrO_2 doping the TZO film can detect ethanol within a short period of time.

Although RF-sputtered binary TZO coatings show promising ethanol sensing, further work is required before practical deployment. Future studies should investigate: time-series sensor response, sensor response versus ethanol concentration (sensitivity curve), selectivity against other gases, dependence on coating thickness, long-term stability, and gas adsorption analysis (e.g., BET) to quantify specific surface area.

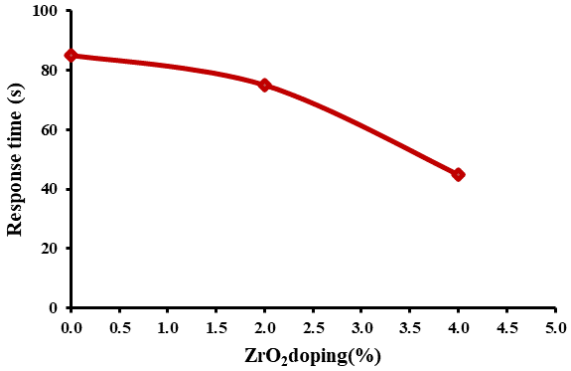

Fig. 9. Response time for TiO_2:ZrO_2 thin films at different dopings

4. CONCLUSSIONS

The structural, morphological, optical and electrical properties of RF magnetron-sputtered TiO_2 films doped with 0, 2 and 4 wt% ZrO_2 were examined. XRD confirmed a polycrystalline anatase structure and the appearance of additional peaks after doping, indicating ZrO_2 incorporation. Average grain size decreased by ~16.6 nm and ~33.2 nm for 2.0 wt% and 4.0 wt% ZrO_2, respectively. Electrical resistivity decreased and carrier mobility increased with ZrO_2 content. The TiO_2:ZrO_2 films with 4.0 wt% ZrO_2 achieved the highest sensitivity (~5.83%/ppm) and the shortest response time (~45 s) for ethanol detection at room temperature. Thus, TZO films with 4 wt% ZrO_2 are promising candidates for ethanol-vapor sensing.

REFERENCES

[1] Jalaukhan, A. H. "Optical investigation of TiO_2/graphene oxide thin film prepared by spin coating technique". IOP Conference Series: Materials Science and Engineering, 2020, 871, 1, 012087.

[2] Sittishoktram. M., E. Ketsombun and T. Jutarosaga, "Optical properties of DC sputtered titanium dioxide/gold thin films", J. Phys: Conf. Series, 2017, 901, 1-4.

[3] Marien CB. D., Marchal, C., Koch, A., Robert, D., Drogui, P., "Sol-gel synthesis of TiO_2 nanoparticles: effect of Pluronic P123 on particle's morphology and photo-catalytic degradation of paraquat", Environ Sci Pollut Res, 2016, 23, 1007-11016-7681.

[4] Rzaij, J. M., & Abass, A., M., "Review on: TiO_2 thin film as a metal oxide gas sensor". J. Chem., Rev, 2020, 2(2), 114-121.

[5] Comert. B, Akin, N., Donmez, M., Saglam,

[DOI: 10.22068/ijmse.3955]

S., and Ozcelik, S., "Titanium Dioxide Thin Films as Methane Gas Sensors.", J. IEEE. Sensor 2016, 16(24), 8890-8896.

[6] Ben Karoui. M, Kaddachi, Z., and, Gharbi, R., "Optical properties of nanostructured TiO_2 thin films", J. Phys: Confe. Seri., 2015, 596, 1-6.

[7] Haidry., A. A., Schlosser, P., Durina, P., Mikula, M., Tomasek, M., Plecenik, T., et al., "Hydrogen gas sensors based on nano-crystalline TiO_2 thin films", J. Cent. Eur. Phys., 2011, 9(5), 1351-1356

[8] Zhang, J., Zhou, P., Liu, J., Yu, J., "New understanding of the difference of photo-catalytic activity among anatase, rutile and brookite TiO_2", J. Phys. Chem. Phys. 2014, 16, 20382–20386.

[9] Ali, H. S., Jasim, R.I, Magid, H.C., Hussein, S., A., Chiad, S., S., Habubi, N., F., Kadhim, Y.H., & Jadan, M., "Influence of thickness on the physical properties of nanostructured TiO_2 thin films for nitrogen dioxide gas sensor", J. Nano. & Bios., 2025, 20, 2, 595-608.

[10] Serga, V., Burve, R., Krumina, A., et al. Study of phase composition, photocatalytic activity, and photoluminescence of TiO_2 with Eu additive produced by the extraction-pyrolytic method", J. Mate. Res. and Tech., 2021, 13, 2350-2360.

[11] Zhao, Q., Wang M., Yang H, Shi D, Wang Y. Preparation, characterization and the antimicrobial properties of metal ion-doped TiO_2 nano-powders, J. Ceram. Inter., 2018, 44(5):5145-5154.

[12] Cetin, S., S., Baleanu, C., M., Nigmatullin, R., R., Baleanu, D., and Ozçelik, S., "Chemical bonding structure of TiO_2 thin films grown on n-type Si", Thin Solid Films., 2011, 519, 16, 5712–5719.

[13] Selmi, M., Chaabouni, F., Abaab, M., and Rezig, B., "Preparation and characterization of TiO_2 thin films grown by RF magnetron sputtering", J. Phys. Status Solidi C., 2008, 5, 10, 3368–3372.

[14] Kadachi, Z., Karoui, M., B., Azizi, T., and Gharbi, R., "Effect of TiO_2 blocking layer synthesised by a sol–gel method in performances of fluorine-doped tin oxide/ TiO_2/dyed-TiO_2/electrolyte/pt/fluorine-doped tin oxide solar cells based on natural mallow dye", Micro Nano Lett. 2016, 11, 2, 94–98.

[15] Sharma, A., K., Thareja, R., K., Willer, U., and Schade, W., "Phase transformation in room temperature pulsed laser deposited TiO_2 thin films", Appl. Surf., Sci. 2003, 206, 137–148.

[16] Mukherjee, S., K., Nebatti, A., Mohtascham, F., Schipporeit, S., Notthoff, C., and Mergel, D., "Influence of thickness on the structural properties of radio-frequency and direct-current magnetron sputtered TiO_2 anatase thin films", Thin Solid Films, 2014, 558, 443–448.

[17] Mohammed Hadi. Shinen, AlSaati, S., A., A., and Fouad Z Razooqi, "Preparation of high transmittance TiO_2 thin films by sol-gel technique as antireflection coating", 2018, J. Physics: Conf. Series, 45678, 012018.

[18] Wall, Staffan., "The history of electrokinetic phenomena". J. Current Opinion in Colloid & Interface Science 15.3, 2010, 119-124.

[19] Bodson, C., J., Heinrichs, B., Tasseroul, L., Bied, C., Mahy, J., G., Wong Chi Man, M., Lambert, S., D., "Efficient P- and Ag-doped titania for the photocatalytic degradation of waste water organic pollutants", J. Alloys Compd, 2016, 682, 144-153.

[20] Mahy, J., G., Paez, C., A., Carcel, C., Bied, C., Tatton, A., S., Damblon, C., B. Heinrichs, B., Lambert, S., D., "Porphyrin-based hybrid silica-titania as a visible-light photocatalyst", J. Phot. Photobi. A Chem., 2019, 373, 66–76.

[21] Leonard, G., L., M., Paez, C., A., Ramírez, A., E., MahyJ, G., Heinrichs, B., "Interactions between Zn^{2+} or ZnO with TiO_2 to produce an efficient photocatalytic, superhydrophilic and aesthetic glass", J. Photo. Photobiol. A Chem. 2018, 350, 32-43.

[22] Wu, M., Leung, D., C., Zhang, Y., Huang, H., Xie, R., Szeto, W., Li, F., "Toluene degradation over Mn-TiO_2/CeO_2 composite catalyst under vacuum ultraviolet (VUV) irradiation", J.Chem. Eng. Sci., 2019, 195, 985–994.

[23] Tian, Q., Wei, W., Dai, J., Sun, Q., Zhuang, Z., Zheng, Y., Liu, P., Fan, M., Chen, L., "Porous core-shell $Ti_xSn_{1-x}O_2$ solid solutions with broad-light response: One-pot synthesis and ultrahigh photooxidation performance", J. Appl. Catal. B Environ., 2019, 244, 45–55.

[24] Mahy, J., G., Lambert, S.D., Tilkin, R., G., Wolfs, C., Poelman, D., Devred, F., Gaigneaux. E., M., Douven, S., "Ambient

[DOI: 10.22068/ijmse.3955]

temperature ZrO_2-doped TiO_2 crystalline photocatalysts: Highly efficient powders and films for water depollution", J. Mate. Today. Ener, 2019, 13, 312-322.

[25] Li, S., GuO, R., Li, J., Chin, Y., and Liu, W., "Synthesis of NiO-ZrO_2 powder for solid oxide fuel cells", Cera. Inter, 2003, 29, 883-886.

[26] Bari, R., H., Patil, S., B., Deshmukh, S., B., "Ammonia Sensing Performance of Nanostructure Cr Doped ZrO_2 Thin Film Deposited by Spray Route", J. Nano. & Techno. 2016, 2 (3), 181-185.

[27] Deshmukh, S., B., Bari, R., "Nanostructured ZrO_2 thin films deposited by spray pyrolysis techniques for ammonia gas sensing application", Phys & Astro. ,2015, 56, 120-130.

[28] Deshmukh, S., B., Bari, R., H., Patil G., E., Kajale, D., D., Jain, G., H., Patil, L., A., "Preparation and characterization of Zirconia based thick film resistor as a ammonia gas sensor", J. Smar. Sensi. Ensin & Intell. Syste. 2012, 5, 3, 540-558.

[29] Simon, S. M., George, G., Sajna, M. S., Prakashan, V. P., Jose, T. A., Vasudevan, P., & Unnikrishnan, N., V., "Recent advancements in multifunctional applications of sol-gel derived polymer incorporated TiO_2-ZrO_2 composite coatings: A comprehensive review", J. Appl. Surf. Sci. Adva., 2021, 6, 100173.

[30] Saleem, A., M., Gnanasaravanan, S., Saravanakkumar, D., Rajasekar, S., Ayeshamariam, A., & Jayachandran, M., "Preparation and characterization studies of TiO_2 doped ZrO_2 on ITO nanocomposites for optoelectronic applications", J. Mate. Tod.: Proc., 2021, 36, 408-415.

[31] Wang, H., Li, Y., Ba, X., Huang, L., Yu, Y., "TiO_2 thin films with rutile phase prepared by DC magnetron co-sputtering at room temperature: effect of Cu incorporation", J. Appl. Surf. Sci., 2015, 345, 49–56.

[32] Sertel, B. C., Sonmez, N. A., Kaya, M. D., & Ozcelik, S., "Development of MgO: TiO_2 thin films for gas sensor applications", J. Cer. Int., 2019, 45(3), 2917-2921.

[33] Madvar, H., R., Kordrostami, Z., and Mirzaei, A., "Sensitivity Enhancement of Resistive Ethanol Gas Sensor by Optimized Sputtered-Assisted CuO Decoration of ZnO Nanorods", J. Sens., 2023, 23, 365.

[34] Simonenko, E.P., Mokrushin, A.S., Simonenko, N.P., Voronov, V.A., Kim, V.P., Tkachev, S.V., Gubin, S.P., Sevastyanov, V.G. and Kuznetsov, N.T., "Ink-jet printing of a TiO_2–10% ZrO_2 thin film for oxygen detection using a solution of metal alkoxo-acetylacetonates", Thin Solid Films, 2019, 670, pp. 46-53.

[35] Miller, T. A., Bakrania, S. D., Perez, V., and Wooldridge, M. S., "Nanosturctured tin dioxide materials for gas sensor applications", J. Func. Nano., 2006, 1–24.

[36] Bilge Saruhan, Roussin Lontio Fomekong, and Svitlana Nahirniak, "Review: Influences of Semiconductor metal Oxide Properties on Gas Sensing Characteristics", Frontiers in Sensors, 2021, 2, 1-24.

[37] Ching-Hua Wei and Ching-Min Chang, "Polycrystalline TiO_2 Thin Films with Different Thicknesses Deposited on Unheated Substrates Using RF Magnetron Sputtering", J. Mate Transactions, 2011, 52, 3, 554-559.

[38] Tian, J., Shao, Q., ZhaoJ., Pan, D., Dong, M., Jia, C., Ding, T., "Microwave solvothermal carboxymethyl chitosan templated synthesis of TiO_2/ZrO_2 composites toward enhanced photocatalytic degradation of Rhodamine", J. Coll. Int. Sci., 2019, 541, 18–29.

[39] O. Abayomi. T, J. Albert O, A. IIona Oja, M. Arvo, and K. Malle, "Effect of Zr doping on the structural and electrical properties of spray deposited TiO_2 thin films", Procee. Eston. Acad. Scie., 2018, 67, 147-157.

[40] Yao, Y., Yuan, J., Chen, X., Tan, L., Gu, Q., Zhao, W., & Chen, J., "In situ construction and sensing mechanism of TiO_2–WO_3 composite coatings based on the semiconductor heterojunctions, J. Mate. Res. Tech., 2019, 8(4), 3580-3588.

[41] Obed, B., G., Hameed, A., S., & Alaaraji, H., H., "Structural and optical properties of TiO_2:MgO thin films preparing at 373k", J. Nano. & Biosts., 2017, 12, 4, 1239-1246.

[42] Chuanzhi, S., Lichen, L., Lei, Q., Hao, L., Z. Hongliang, L. Changshun, G. Fei, D. Lin, "Efficient fabrication of ZrO_2-doped TiO_2 hollow nanospheres with enhanced photocatalytic activity of rhodamine B degradation", J. Coll. & Inte. Scie., 2011, 364, 288-297.

[43] Abdulmunem, O., M., Jabbar, A., M., Muhammad, S.K., Dawood, M., O., Chiad,

[DOI: 10.22068/ijmse.3955]

S., S., Habubi, N., F., 2020, J. Phy.: Conf. Ser., 1660 (1), 012055.
[44] Sun, C., Liu, L., Qi, L., Li, H., Zhang, H., Li, C., Gao, F., & Dong, L., "Efficient fabrication of ZrO_2-doped TiO_2 hollow nanospheres with enhanced photocatalytic activity of rhodamine B degradation", J. Coll. & Inter. Scie., 2011, 364, 288–297.
[45] Schiller R., Weiss. C. K, and Landfester. K., "Phase stability and photocatalytic activity of Zr-doped anatase synthesized in miniemulsion", J. Nano. techno., 2010, 21, 405603(1-11).
[46] Ali, H., S., Jasim, R., I., Magid, H., CH., Hussein, S., A., Chiad, S., S., Habubi, N., F., Kadhim, Y., H., M. Jadan, M., "Influence of thickness on the physical properties of nanostructured TiO_2 thin films for nitrogen dioxide gas sensor", J. Nano. & Bio., 2025, 20, 2, 595-608.
[47] Sreemany, M., Bose, A., & Sen, S., "A study on structural, optical, electrical and microstructural properties of thin TiOx films upon thermal oxidation: Effect of substrate temperature and oxidation temperature", Physica B, 2010, 405, 85-93.
[48] Sakhil, M., D., Shaban, Z., Sharba, M., K., S., Habubi, N., F., Abass, K., H., Chiad S., S., Alkelaby, A., S., J. Neu. Quan., 2020, 18(5), 56-61.
[49] Bedikyan, L., Zakhariev, S., Zakharieva, M., "Titanium dioxide thin films: preparation and optical properties", J. Cheml. Techn. & Metal., 2013, 48, 6, 555-558.
[50] Lang, J., Matejová, L., Troppova, I., Capek, L., Endres, J., & Danis, S., "Novel synthesis of $Zr_xTi_{1-x}O_n$ mixed oxides using titanyl sulphate and pressurized hot and supercritical fluids, and their photocatalytic comparison with sol-gel prepared equivalents", J. Mater. Res. Bull. 2017, 95, 95–103.
[51] Neppolian, B., Wang, Q., Yamashita, H., Choi, H., "Synthesis and characterization of ZrO_2-TiO_2 binary oxide semiconductor nanoparticles: Application and interparticle electron transfer process", J. Appl. Catal. A Gen., 2007, 333, 264–271.
[52] Devia, S., R, P. J. Saikiab, Hussainc, M., A., "Studies on optical and electrical properties of PVA capped nanocrystalline CdSe thin film prepared by chemical bath deposition method", 2022, J. Chalcogenide Lett., 2022, 19, 12, p. 901–908.
[53] Brik, M. G., Srivastava, A. M., & Popov, A. I., "A few common misconceptions in the interpretation of experimental spectroscopic data", J. Optical Materials, 2022, 127, 112276.
[54] Boonyopakorn N, Rangkupan R, Osotchan T., "Synthesis of TiO_2/Fe_2O_3 composite material derived from ilmenite ore for photocatalytic degradation of malachite green dye", J. Sci. Techno, 2018, 40(4), 824-830.
[55] Mokrushin, A. S., Simonenko, E. P., Simonenko, N. P., Bukunov, K. A., Gorobtsov, P. Y., Sevastyanov, V. G., & Kuznetsov, N. T., "Gas-sensing properties of nanostructured $TiO_{2-x}ZrO_2$ thin films obtained by the sol–gel method", J. Sol-Gel Sci. & Tech., 2019, 92, 415-426.
[56] Huang, Z., Wang, W., Xiao, D., Mo, Y., Wang, S., Xu, Z., & Peng, J., "Ethanol gas sensing with lower temperature and higher response based on three-dimensional multilevel materials composed of micron hollow carbon spheres@SnO_2 nanoparticles", Mate. Today Comm., 2022, 32, 104105.
[57] Patil, L., A., Sonawane, L.S., D.G. Patil, D., G., "Room temperature Ammonia gas sensing using MnO- modified ZnO thick film resistors", 2011, J. Mod. Phys., 2, 1215.
[58] L. A. Patil, L.S. Sonawane, D.G. Patil, "Room temperature Ammonia gas sensing using MnO- modified ZnO thick film resistors", 2011, J. Mod. Phys., 2, 1215.

[DOI: 10.22068/ijmse.3955]